OPEN ACCESS

University of BRISTOL

Wrobel, R., Simpson, N., Mellor, P., Goss, J., & Staton, D. (2016). Design of a brushless PM starter-generator for low-cost manufacture and a high-aspect-ratio mechanical space envelope. In 2015 IEEE Energy Conversion Congress and Exposition (ECCE 2015): Proceedings of a meeting held 20-24 September 2015, Montreal, Quebec, Canada. (pp. 813-820). (Proceedings of the IEEE Energy Conversion Congress and Exposition (ECCE)). Institute of Electrical and Electronics Engineers (IEEE). 10.1109/ECCE.2015.7309773

Peer reviewed version

Link to published version (if available):
10.1109/ECCE.2015.7309773

Link to publication record in Explore Bristol Research
PDF-document

Design of a Brushless PM Starter-Generator for Low-Cost Manufacture and a High-Aspect-Ratio Mechanical Space Envelope

Rafal Wrobel, Nick Simpson, Phil H. Mellor
Department of Electrical & Electronic Engineering
University of Bristol, Bristol, UK
r.wrobel@bristol.ac.uk
nick.simpson@brsitol.ac.uk
p.h.mellor@brsitol.ac.uk

James Goss, Dave A. Staton
Motor Design Ltd., Ellesmere, UK
james.goss@motor-design.com
dave.staton@motor-design.com

Abstract — **This paper presents results from a design study into a brushless PM starter-generator. The automotive application demands a low-cost solution within a highly constrained mechanical space-envelope. Material costs are reduced through the use of ferrite permanent magnets and aluminium conductors. Design challenges include the selection of an appropriate machine topology to realise a high specific output given the lower performance materials and managing the additional losses associated with the higher resistivity of an aluminium winding. The problem is further exacerbated by the demanding space-envelope, operating requirements and the necessity of a design suited to volume manufacture. The packaging arrangement suits an internal-rotor radial-flux topology and the limited mechanical space-envelope means that the aspect ratio of the stator outer diameter to the machine active length is high. The design approach outlined in the paper combines numerical electromagnetic analyses with a lumped parameter thermal model and is calibrated with tests on machine subassemblies. The methodology allows for a more informed design process, where the manufacture and assembly nuances affecting the performance of the starter-generator are identified and accounted for prior to the prototyping of a complete machine assembly.**

Keywords—PM starter-generator, design for manufacture, design for cost, low-cost aluminium winding, ferrite PM rotor, manufacturing variations;

I. INTRODUCTION

The design of electrical machines is a multi-disciplinary problem in which the various performance requirements such as torque-speed envelope, duty-cycle and thermal characteristics should be considered alongside specific design paradigms such as 'design for cost' or 'design for manufacture'. The various design drivers limit the range of applicable solutions and the full breadth of requirements needs to be captured at an early stage in the design process. The literature reflects an increased interest in incorporating cost and manufacturability considerations in the design synthesis of electrical machines [1]-[12]. For example a recent focus has been towards designs with reduced reliance on rare-earth PM materials, prompted by concerns over supply and price volatility. Proposed solutions include the adoption of interior PM machine topologies or the use of alternative PM materials such as ferrites, Dysprosium-free or Dysprosium-less NdFeB. Furthermore, PM-free designs such as reluctance and synchronous reluctance machine topologies have received considerable attention [1]-[5]. Alternative low-cost stator and winding topologies have been reported which are more suited to low cost manufacture and assembly without unduly compromising performance measures such as good heat extraction from the winding assembly and low loss [6]-[12].

This paper presents findings from a design study on a brushless PM starter-generator. The 'design for cost' and 'design for manufacture' considerations are included through the use of less expensive active materials and the adoption of simple manufacturing and assembly method for stator winding. The selected topology is a radial-flux machine with an open-slot stator structure accommodating pre-formed aluminium windings and an inner rotor with surface mounted ferrite PMs. The incorporation of the lower cost materials, which exhibit poorer magnetic and electrical properties, is likely to compromise the achievable machine performance within a given space-envelope. Redefining the packing constraint may add additional cost to overall system, offsetting any savings made in the electrical machine. This leads to a challenging design brief.

A co-design methodology based on theoretical and experimental techniques has been adopted. Numerical finite element analyses are used to identify electromagnetic parameters and loss effects. Functional relationships are employed to predict the manner in which these losses vary with machine operating point and temperature. In tandem a lumped-parameter thermal model is used to estimate operating temperatures, coupled to the loss functions. Model parameters are calibrated through experimental tests on machine hardware subassemblies (motorettes). In particular these motorette experiments provided valuable insight into how manufacture and assembly nuances can impact the stator winding loss and cooling. An overview of the design process supplemented with experimental and theoretical data is provided in consecutive sections of the paper. A number of candidate winding constructions are compared. The theoretical analyses and

results from the motorette hardware tests highlight some of the challenges of using preformed aluminium coils.

II. DESIGN PHILOSOPHY

A major consideration in the initial choice of a modular wound, radial-flux machine topology with an open parallel sided stator slots is the requirement for simple winding manufacture and assembly. In principal the single layer concentrated winding topology allows for the coils to be manufactured in isolation in a simple and repeatable manner. The preformed coils are then placed in the stator slots with an appropriate slot liner and secured with a slot wedge. The complete stator-winding assembly is then impregnated with varnish, which serves to provide the electrical insulation and mechanical integrity. The arrangement also allows a high volume of conductor to be incorporated in the stator design.
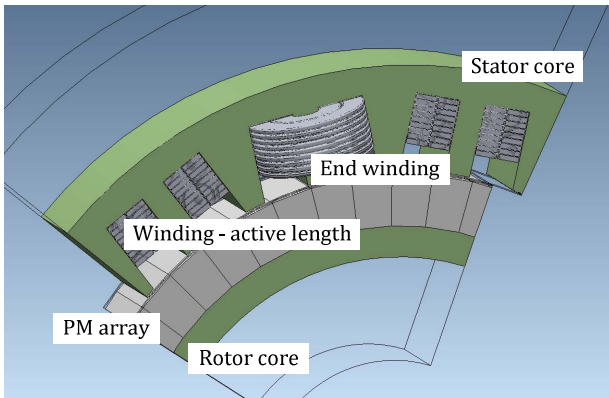

Fig. 1. Section of the starter generator geometry

TABLE I. OUTLINE MOTOR SPECIFICATION

Package volumetric envelope	3.6 litres
Maximum rated rotational speed	5000rpm
Nominal power/torque (continuous)	7.5kW/30Nm
Peak transient power/torque	15kW/60Nm
Nominal voltage	48V

The design is based on a variant of a 10 pole (p =10) 12 slot (q = 12) machine topology with a single-layer, three-phase concentrated winding, Fig. 1. Table I lists the motor specification including the output power requirements and the space-envelope restrictions. The outer diameter to length aspect ratio is 9.4. The target magnetic and electrical loadings which satisfy the output requirements were set to B_I=0.4T and Q_{rms}=70,000A$_{rms}$/m respectively. These loading values are demanding when considering the properties of readily available low cost ferrite permanent magnets and the higher resistance of aluminium conductors. The limited active area combined with the relatively low magnetic loading leads to a target electric loading comparable to more conventional copper wound machine designs and consequently a large number of Ampere-Turns per phase. The winding and core losses are additionally affected by the relatively high operating fundamental frequency, equal to approximately 1kHz at the high-end of the required torque-speed envelope. Furthermore, the phase inductance has to be constrained within a limited range to ensure the required peak power at higher operating speeds within the inverter supply constraints. Therefore, in order to realise a feasible machine design each of the performance issues must to be addressed concurrently.

The choice of modular 10-12 topology allows for a large slot winding area and preformed coils. The active volume available to the winding is much higher than for more conventional distributed windings. The arrangement of conductors within the stator slots has been defined to minimise ac effects and coil compression is employed to maximise the conductor fill factor, k_p. Thin 0.2 mm SiFe laminations are used to form the stator pack to reduce eddy-current loss at high-speed operation. In order to fully utilise the lower grade PM material and provide the required magnetic loading, a two-segment per pole discrete-Halbach PM array is adopted. Despite the large permeance variations associated with the open slot stator the PM eddy current loss was found to be negligible due to the high electrical resistivity of the ferrite material. Careful considerations must be made when designing a ferrite PM rotor array to avoid demagnetisation which can result from high electric loading combined with low temperatures which are likely to occur in the present application.

Fig. 1 presents a schematic of the active elements, and illustrates the relatively short active length of the machine and the large end-windings of the preformed concentrated winding. A parallel-sided slot design is introduced to simplify the manufacture and assembly of the winding and to improve the heat transfer from the winding body into the stator and housing assembly. Good thermal contact is particularly important as the machine housing is interfaced with a water jacket which provides the main extraction path for the generated power loss.

III. MACHINE PROTOTYPING

One of the vital components in the development of the starter-generator is the winding assembly. A number of coil constructions have been evaluated with respect to the generated loss and ease of manufacture. These include an edge-wound coil construction with profiled rectangular conductors, winding variant I and a multi-stranded round conductor construction in uncompressed and compressed forms, winding variants II and III respectively, Figs. 2a, 2b and 2c. Fig. 2d presents a prototype of the multi-stranded and compressed coil that has been in cross section revealing a high degree of conductor compaction, with the individual conductor's cross-section being deformed from a circular cross-section to a polygonal shape [12]. The winding variant I provides the highest conductor fill, k_p , equal to 76%. Here the conductor fill factor is defined as a ratio of the total conductors' cross-section to the available winding window cross-section. This differs from the more commonly used definition, where the entire stator slot cross-section is used as a reference. The alternative definition has been adopted due to the specifics of the winding construction, where the stator slot is intentionally partially filled by conductors.

Winding variants II and III have a lower conductor fill factor and consequently a higher dc resistance. Conductor fill factor is not necessarily indicative of the winding loss over the full range of operating speeds (frequencies) as ac loss effects can be dominant [14]. In the case of variants II and III the

winding is formed from a number of smaller gauge parallel conductors per turn. In principal a multi-stranded bundle will have lower ac eddy current losses, provided the characteristic dimensions of the individual conductors are less than the conductor skin depth. Rotational ac loss effects occur as a result of slot leakage fluxes induced by the passing magnets on the rotor and have been shown to be particularly significant for open-slot stator designs [14]. To further reduce the rotational ac power loss component, the winding body is placed lower in the stator slots and occupies approximately 80% of the complete slot depth/window.
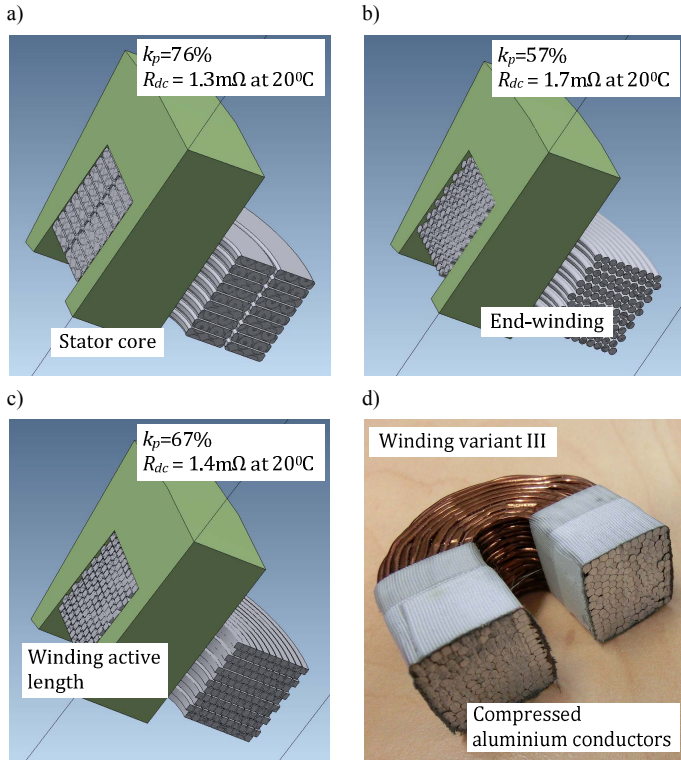

Fig. 2. Outline of the winding's coil constructions a) 1.9mm×8.3mm edge wound – winding variant I, b) 6×∅1.6mm multi-stranded wound –winding variant II, c) 7×∅1.6mm compressed multi-stranded wound –winding variant III, d) cross-section of a prototype coil with compressed conductors

A drawback of a multi-stranded winding is that the positioning of the individual strands in the coil is somewhat random. The undefined conductor placements makes the analysis of ac loss effects difficult and may results in a differing level of the loss in the individual coils which make up the winding [15]. This effect is explored in more detail in the Section V of the paper.

IV. ANALYSIS OF WINDING LOSS

Electromagnetic and thermal analyses have been performed in order to establish the feasibility of the proposed design. Electromagnetic finite element analysis (FEA) was employed to define the dimensions of the stator iron and the magnet array. This FEA was also used to set the winding turns and to establish the machine torque constant, emf and inductance. Further it was used and to investigate in more detail the distribution of loss in the stator and rotor. A lumped-parameter thermal equivalent-circuit model was formulated to

assess the thermal behaviour of the design over the required operating cycle, using the FEA derived loss data as input. The stator loss and thermal analysis is the focus of this this section.

The initial FEA confirmed that the open-slot stator-winding arrangement is susceptible to elevated ac loss effects. To mitigate for rotational ac losses induced by the PM excitation the winding height was restricted to the back of the slot, Figs. 1 and 2. Whilst this limits the available conductor cross-section area, increasing the coil dc resistance, the overall loss across the operating cycle is reduced.

A. Winding Loss Model

Two- and three-dimensional (2D and 3D) FEA of the winding variants discussed earlier have been carried out. Ac winding loss calculations have been performed using time stepping FEA assuming an ideal 3-phase sinusoidal current excitation of the windings. The individual winding's conductors are represented within the FE model as solid conductors linked with an external circuit defining electrical connections between the winding conductors, coils and phases where appropriate. To emulate random conductor lay for the winding variants II and III an irregular shape of bundles forming the individual winding's turns has been assumed as shown in Fig. 3. It is important to note that no transposition of the individual stands has been considered, i.e. all conductors are geometrically parallel in the plane of the coil winding.
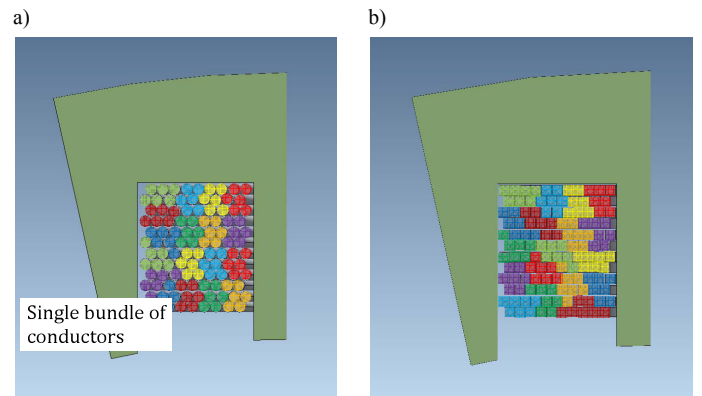
Fig. 3. Conductor's lay assumed in the FEAs a) winding variant II, b) winding variant III

The short active length and the single-layer modular coil construction meant that the end-turn and active regions of the winding were of comparable length. Whilst a 2D FEA was sufficient to cater for the active region of the machine, a 3D FEA model of a single coil and slot assembly was needed to estimate the end-winding contribution to the coil loss and inductance. The total winding loss is a sum of the active length and end-winding components:

$$P_{ac} = P_{ac\ al} + P_{ac\ ew} \qquad , \qquad (1)$$

where $P_{ac\ al}$ and $P_{ac\ ew}$ refer to the active length and end-winding region losses under ac operation respectively.

This decoupled approach allows for the winding loss to be derived in a computationally efficient manner. Symmetry can be exploited to reduce the 3D FE model to that of half an end-turn and the number of 3D FEA computations are kept to a

minimum. Rotor induced ac loss effects in the end-winding region are assumed to be negligible.

In the FEA, the generated winding loss is calculated from the Joule loss in the conductor regions [14]. To account for the change in conductor resistivity with temperature, the established linear correction has been used:

$$\rho|_T = \rho|_{T_0}\big(1 + \alpha(T - T_0)\big) \qquad , \qquad (2)$$

where $\rho|_{T_0}$ is the resistivity of aluminium conductors at $T_0 = 20°C$, $2.83×10^{-8}\Omega m$, and α is the temperature coefficient of resistance for aluminium is $4.3×10^{-3}$ C^{-1}. The FEA assumes a constant conductor temperature T across the winding body.

The winding loss data obtained from a reduced number of FEAs has been used to inform the coefficients of a winding loss function for both the active length and end-winding regions. The functional representation of the winding power loss proposed in [14] has been employed and accounts for the manner the loss varies with temperature and frequency:

$$P_{ac}|_T = P_{dc}|_{T_0}\big(1 + \alpha(T - T_0)\big)$$

$$+P_{dc}|_{T_0}\frac{\left(\frac{R_{ac}}{R_{dc}}\right)_E\Big|_{T_0} - 1}{\big(1 + \alpha(T - T_0)\big)^\beta} \qquad , \qquad (3)$$

$$+P_{acR}|_{T_0}\frac{1}{\big(1 + \alpha(T - T_0)\big)^\gamma}$$

where:

$$P_{dc}|_{T_0} = I^2 R_{dc}|_{T_0} \qquad , \qquad (4)$$

$$\left(\frac{R_{ac}}{R_{dc}}\right)_E\Big|_{T,I} = \left(\frac{P_{ac} - P_{acR}}{P_{dc}}\right)\Big|_{T,I} \qquad , \qquad (5)$$

R_{dc} is the winding dc resistance. $(R_{ac}/R_{dc})_E$ is the ac loss factor defines the ratio of the ac winding loss to the dc winding loss at a given winding temperature, T, and current, I [16]. P_{acR} is the rotor induced winding loss for open-circuit operation. The ac loss factor can be derived from electromagnetic FEA or test measurement. The temperature indices β and γ are found by fitting (3) to FEA ac loss calculation performed over the expected upper and lower operating temperatures. Their values for the three winding variants are listed Table II. As it is assumed rotor induced losses are negligible in the end-winding the related temperature index γ_{ew} is not relevant. A value of β, γ=1 is commensurate with an induced voltage driven resistance limited eddy current problem where the ac

TABLE II. FEAs' DERIVED COEFFICIENT FOR THE POWER LOSS FUNCTION

Winding variant	Active length region		End-winding region	
	β_{al}	γ_{al}	β_{ew}	γ_{ew}
I	0.90	0.50	0.60	-
II	0.75	1.00	0.80	-
III	0.75	1.00	0.80	-

loss is inversely proportional to the effective resistance of the eddy current path. With relatively large cross section conductors, such as winding variant I, the eddy current pattern becomes increasingly inductance limited and is therefore less

sensitive to the temperature variation of the path resistance. Since (3) maps the winding loss variation with operating frequency, current amplitude and temperature, it can be readily used to derive a loss/efficiency map over the design torque-speed envelope or a particular operating duty-cycle.

The iron loss in the stator core pack was estimated from the electromagnetic FEA based on the modified Steinmetz loss formulation. The required hysteresis, eddy current and excess loss coefficients were found from the manufacturers' specific loss data for the 0.2mm thick SiFe laminates used. To minimise the number of computations a similar process to the winding ac loss has been employed, where the FEA calculations are used to find the coefficients of a polynomial function describing the iron loss variation with current amplitude, current angle and frequency [17]. Since the machine is to be integrated within an engine transmission the mechanical losses have not been considered here.

B.   Thermal Model

A lumped-parameter thermal model for the starter-generator design has been built using a commercially available tool [18]. The model accounts for conduction heat transfer within the stator and rotor elements and the heat exchange through convention into the water cooling circuit and air regions. Fig. 4 presents the thermal network use. The horizontal and vertical circuit-branches represent axial and radial heat paths within the machine assembly respectively. The model utilises periodic symmetry over the machine's circumference in that only a single slot is modelled, i.e. the loss and temperature of each modular coil is assumed identical.

The loss data input to the thermal model is coded in the form of the functional relationships discussed in the previous section. To provide a degree of calibration to the thermal model experimental measurements have been carried out on winding amalgam material samples and a motorette assembly. The aim of these tests was to accurately derive thermal material properties representative of the winding region and to determine the quality of the conductive heat transfer path from the winding into the stator core pack and housing. Details regarding the experimental setups used in the analysis are provided in the next section.

Fig. 4. Thermal lumped-parameter equivalent circuit model representation of the starter-generator assembly

a)

Polymer coated wire
$k_p = 55\%$
$k = 2.3\text{W/mK}$

b)

Oxide coated wire
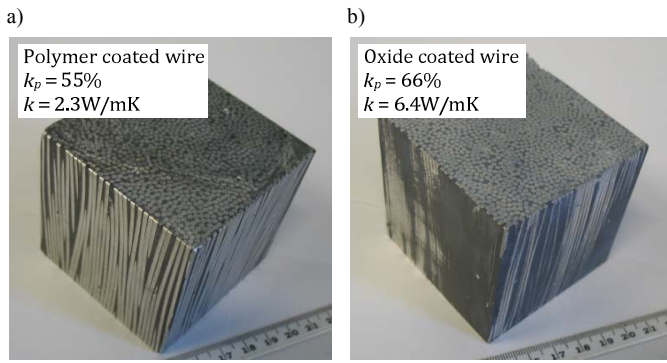$k_p = 66\%$
$k = 6.4\text{W/mK}$

Fig. 5. Impregnated winding material samples representative of the multi-stranded coil construction used to measure thermal properties for the winding amalgam

An initial sensitivity analysis was performed using the thermal model to identify the main heat transfer paths and mechanisms. The analysis confirmed that the dominant heat flow is from the impregnated stator-winding assembly to the liquid cooled housing via the stator core. As a result correct calibration of the interface thermal resistances between the stator-winding and core pack and between the core pack and the machine housing were found to be crucial to the accuracy of the thermal model.

C. Subassembly Hardware Tests

1) Winding Thermal Material Data Derivation

The lumped-parameter thermal model uses an averaged equivalent value of thermal conductivity and specific heat capacity to represents the composite winding region. In order to obtain accurate values for these parameters a number of winding bundle samples have been experimentally characterised. Fig. 5 presents some of the winding samples considered. The test samples comprise cubes formed with alternative wire coatings, impregnation varnishes and varying conductor fill factor. The test procedure uses a heat flux meter to determine equivalent directional thermal conductivities accounting for the winding amalgam anisotropy [19]. The averaged specific heat capacity has been found from calorimetric tests on the winding samples.
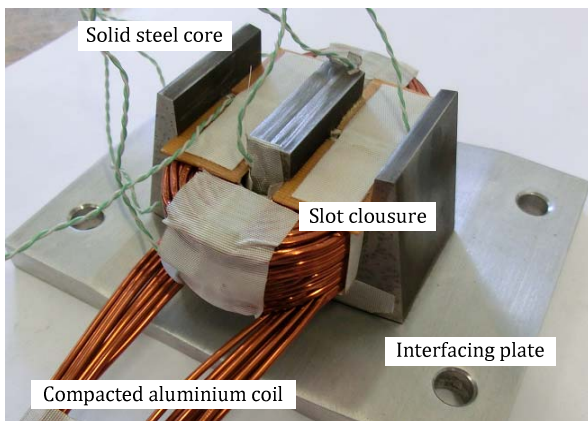
Fig. 6. Instrumented sector of the stator-winding assembly (motorette) prior to impregnation

2) Heat TransferAnalysis

A motorette representative of the coil and tooth arrangement was constructed to calibrate interface thermal resistances. Fig. 2 shows the motorette arrangement prior to final impregnation with varnish. The motorette body was mounted on a liquid-cooled aluminium interfacing plate with appropriate retention system to emulate the housing assembly. The motorette setup was then placed in a thermally insulated chamber and instrumented with type-K thermocouples. The heat input to the motorette winding is provided by a dc power supply, and the temperature of the cold plate is maintained at a constant set-point using an external cooling unit. Thermal resistances were derived from the measured temperature gradients between the winding and core and between core and housing interface. The experiment was repeated over a range of injected loss and temperatures, and the averaged test data was used to calibrate the thermal model.

3) Power Loss Measurements

A precision impedance analyser was used to characterise the inductance and ac loss factor of the manufactured stator coils. The impedance analyser provides an equivalent resistance for the coil at the test frequency, for which the $(R_{ac}/R_{dc})_E$ ac loss factor can be easily derived. Fig. 7 presents the testing setup showing a coil under test positioned in the laminated stator core pack.
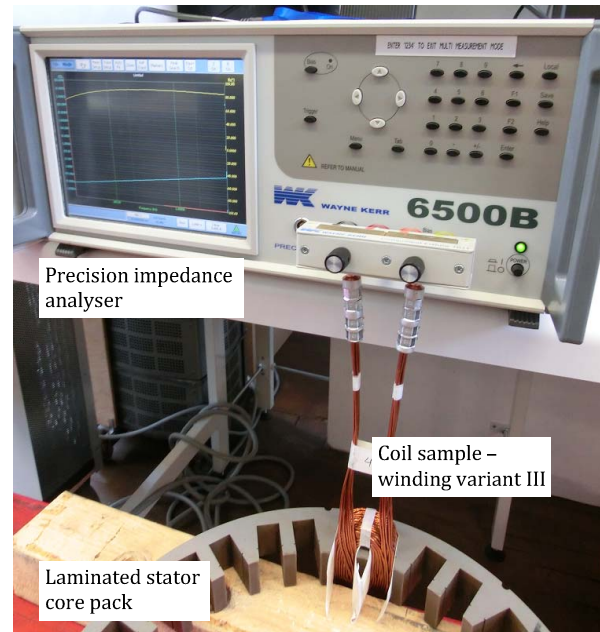

Fig. 7. Experimental setup used to evaluate ac excitation loss and winding inductance

V. COMPARISON OF THE WINDING VARIANTS

The prototyping efforts have been focused on the winding construction with compacted conductors (winding variant III) as a high fill factor could be achieved with a lower ac loss multi-stranded conductor arrangement. The experimental results included in this section are therefore limited to the winding variant III only. Model based analyses have been used to assess the comparable performance of the other winding arrangements.

Initial measurements were focused on confirming the winding inductance lies within the design limits as this determines the maximum power output capability of the starter-generator at high operating speeds. Too low inductance would mean excessive d-axis current during field weakening, too high inductance would mean the peak power would not be achievable. The machine topology has a relatively short active length and the contribution of end-winding will be significant, the 3D FEA analyses suggest that the end-winding inductance is 45% of the overall winding inductance. Whilst the measurements have been confined to the stator winding assembly only, the additional inductance due to the presence of the rotor structure is likely to be small as the depth of the low permeability magnet array is large.

Fig. 7 presents the measured inductance across a batch of eight compressed aluminium coils. A significant variation in the measured coil inductances were observed, ranging from 58µH to 64µH, and are a result of the random nature of the conductor lay in each coil. In the manufacture of the multi stranded coils the conductor turns were wound 'in-hand' and then compressed, with no specific control over the final positioning of the individual aluminium wire strands. A large variation in the individual coil inductance is undesirable as this could lead to circulating current within the parallel coils used to form each phase winding. The average coil inductance for the batch and the FEA derived inductance are also plotted on the figure. The original FEA design predictions are within 10% of the measured average. The inductance is also observed to reduce with frequency and is indicative of ac eddy current effects in the winding [20]. The FEA calculation is equally able to identify the inductance frequency trend. The change in inductance is however negligible across the 0-~1kHz operating frequency range of the machine.

Fig. 8 presents the test measured ac loss factor, $(R_{ac}/R_{dc})_E$, versus frequency for eight sample coils. The measurements were taken at an ambient temperature of ~20°C. The average of measurements and the FEA predictions are also shown. The results indicate large differences between the coils with $(R_{ac}/R_{dc})_E$ values ranging from 3.6 to 6.8 at 1kHz.
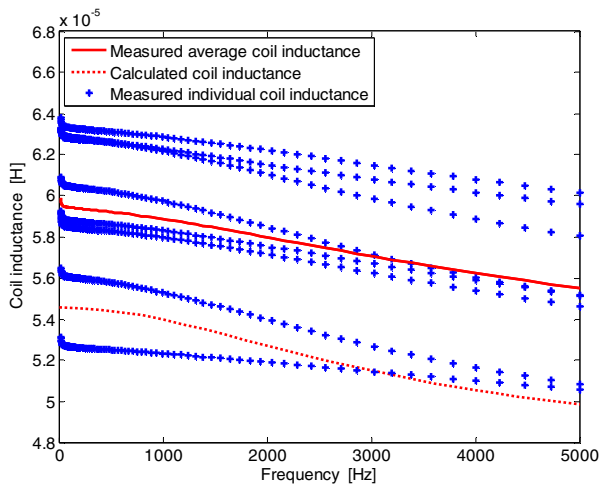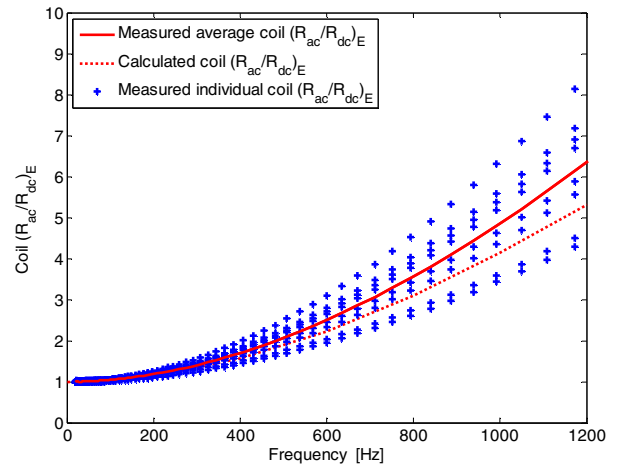

Fig. 8. Measured and calculated $(R_{ac}/R_{dc})_E$ for the individual winding's coils vs. excitation frequency for winding temperature T = 20°C

A potentially wide ranging variation of loss across the winding coil clearly has important implications regarding the machine's thermal performance. It is evident that an improved and more repeatable manufacture process for the multi-stranded compacted winding is needed.

The FEA prediction of the $(R_{ac}/R_{dc})_E$ ac loss factor is close to the average of the experimental findings. This suggests that the proposed FEA based approach is accurate and can be used to compare the performances of alternative conductor arrangements. Fig. 9 compares the FE predicted ac loss factor for the winding variants considered in the paper. The results are separated into values for the winding active $(R_{ac}/R_{dc})_{E\ al}$ and end $(R_{ac}/R_{dc})_{E\ ew}$ regions, which are of similar length. The results suggest that excitation related ac losses of the rectangular conductor winding, variant I, is around half that of the others windings, as well as benefitting from a high conductor fill factor. The calculated ac loss factors in the stranded winding variants II and III are similar. Although the ac loss effects are greatest in the active region the ac end-winding effects are not negligible and need to be accounted for to provide accurate power loss predictions.
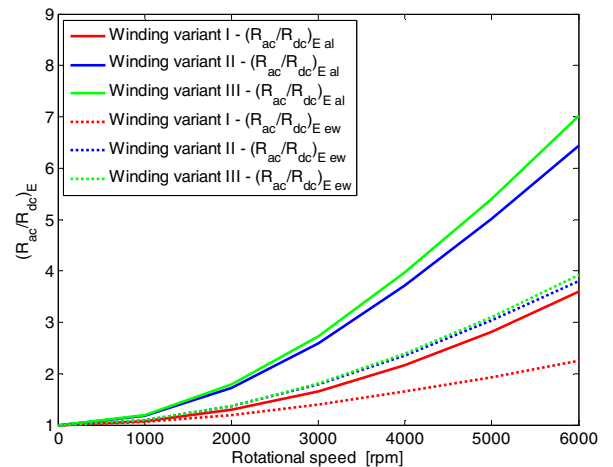

Fig. 8. Measured inductance for the individual winding's coils vs. excitation frequency for winding temperature T~20°C

Fig. 9. Calculated $(R_{ac}/R_{dc})_E$ for the active length and end winding regions vs. rotational speed at winding temperature T = 20°C and I_{ph} = 400A$_{rms}$
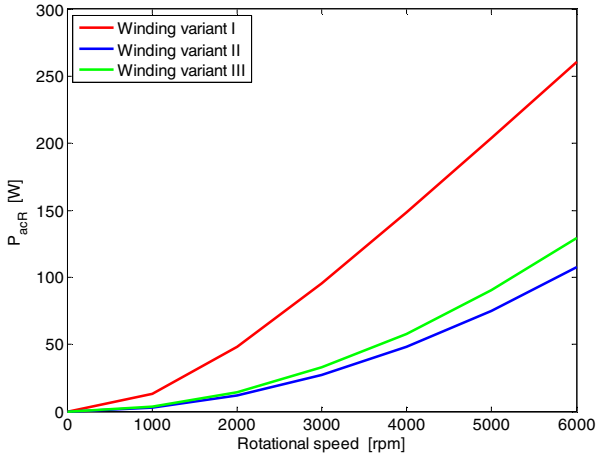
Fig. 10. Calculated winding open-circuit power loss P_{acR} vs. rotational speed at winding temperature $T = 20^0$C

Fig. 10 plots the FEA determined rotor induced winding ac losses for open-circuit operation, P_{acR}. These losses are now greatest for the rectangular conductor winding, variant I, and are around 2.5 times than those of the coils formed from multiple relatively small diameter conductors. The rotor induced loss is greatest in the conductors lying close to the slot opening and the induced eddy currents would be substantial in a large section conductor.

The overall winding loss balance will depend on the desired torque-speed characteristics and duty cycle with stator excitation induced, Fig. 9, and rotor induced, Fig. 10, ac effects contributing differently for lower-speed high-torque and high-speed low-torque operation. Clearly, in order to down select the most promising low-loss winding candidate, an analysis of the complete operating envelope including the intended operating duty is required. Using the methods described earlier in the paper the machine losses have been calculated over a range of torques and speeds and an efficiency map generated. A fixed winding temperature equal 120^0C has been assumed in generating the maps. The combined loss and thermal models have been used to estimate the continuous operating envelope of the design. Here a casing temperature of 65^oC and a maximum winding temperature equal to 160^oC have been imposed.

Fig. 11 compares the results for the winding formed from rectangular conductors, variant I, and that of the compressed multi stranded coil, variant III. Both of these windings exhibit large aluminium fill factors, 76% and 67% respectively and have similar dc resistances. However as indicated in Figs 9 and 10 the two windings will have distinctly different ac loss characteristics. Further the manner in which the ac loss varies with temperature also differs, Table II. The continuous output capabilities of the two alternatives appear to be similar and both meet the application requirements. The rectangular conductor winding has improved continuous power capabilities at high speed as a result of a lower level of stator induced ac loss. The efficiency maps for the two machines are however distinctly different. This is a result of the changing balance of ac loss effects across the operating envelope. The final selection of the winding would be based on the expected operating duty and volume manufacture considerations.
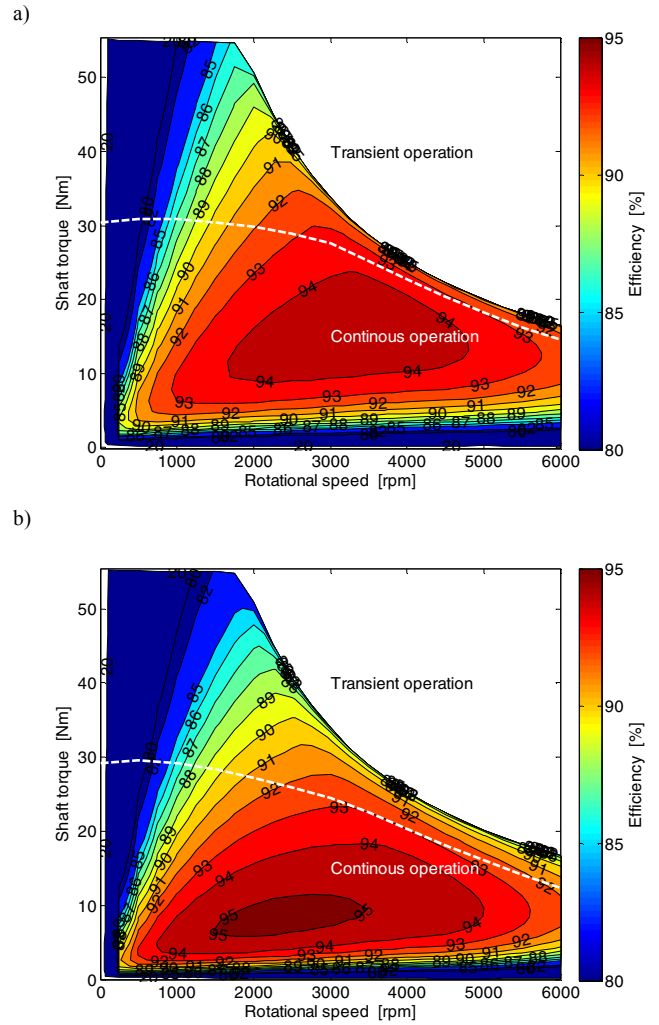
a)

b)

Fig. 11. Estimated machine continuous torque-speed envelope and efficiency map; a) winding variant I, b) winding variant III

VI. CONCLUSIONS

This paper presents results from a study on an integrated brushless PM starter-generator. The original design remit was to incorporate cost effective materials and simple manufacturing and assembly methods. The selected topology is a radial-flux machine with an open-slot modular aluminium winding and an inner rotor with surface mounted ferrite PMs. A Halbach array is used in the rotor construction to realise a relatively high magnet loading, 0.4T, from the ferrite magnets. The open-slot single layer modular topology allows for the coils to be pre-formed and high a volume of conductor can be incorporated to offset the poorer resistance of aluminium. As a result the achieved electrical loading is comparable to that of a more conventional distributed winding using copper conductors.

The employed analyses process used in the design combine theoretical and experimental approaches. 2D and 3D electromagnetic FEA has been employed to define the dimensions of the stator iron and the magnet array. This FEA was also used to set the winding turns and to establish the machine torque constant, emf and inductance. 3D FEA was necessary to appraise the contribution of the end winding; the

contribution of the end winding to the overall inductance and loss is significant due to a short active length. Further the electromagnetic analyses were used to investigate in more detail the distribution of loss in the stator with an emphasis on ac winding loss effects. Functional relationships are used to capture the variation of loss with temperature and operating frequency. This methodology has the benefit of reducing the number of FEA required to characterise the design over a full operating envelope to those required to identify the coefficients in the loss expressions. A lumped-parameter thermal equivalent-circuit model was formulated to assess the thermal behaviour of the design over the required operating cycle, using the FEA derived loss data as input. The resultant coupled electromagnetic and thermal analysis have been applied to determine the continuous output capability within the winding, the thermal constraints and to yield an efficiency map. The initial experimental work used thermal tests on sub-assembly 'motorettes' to calibrate the thermal model. The bulk thermal properties of the winding regions were obtained using heat flux and calorimetric measurements. The thermal resistances across the critical interfaces between the winding and core pack and from the core pack to casing were also estimated from experiment. Electrical tests on the preformed coils were also undertaken. The initial results have shown close correlation between FEA calculated inductances and ac loss factor and measured data. The use of sub-assemblies to calibrate and validate the modelling work is proven to be a valuable and cost effective approach.

The performances of three alternative winding constructions have been compared, one formed from edge wound rectangular conductors, one from multiple strands of parallel conductors and a third compressed version of the multi-stranded arrangement. A high conductor fill factors was achieved in the compressed multi-stranded coils, being only 10% less than that of an ideal rectangular conductor arrangement. The analyses indicated that the rectangular and compressed multi-stranded coil constructions would deliver the required performance of the application, whereas an un-compressed multi-stranded coil construction would not. The ac loss resulting from rectangular and the multi-stranded coils are shown to be very different, the 'edge wound' rectangular conductors have the lowest excitation related ac loss, whereas the multi-stranded arrangements has much lower rotor induced loss.

Experimental measurements on the compressed multi-stranded coil construction indicated that the ac losses, and to a lesser extent the inductance, is highly sensitive to the conductor lay. Tests across a batch of eight coils indicated an ac loss factor spread between 3.6 to 6.8 at 1kHz and an approximately 20% variation in inductance. The random nature of the 'in-hand' method of winding parallel conductor turns means that the conductor lay cannot be precisely defined and a controlled conductor placement method of manufacture is required in the future.

REFERENCES

[1] S. J. Galioto, P. B. Reddy, A. M. El-Refaie, "Effect of Magnet Types on Performance of High Speed Spoke Interior Permanent Magnet Machines Designed for Traction Applications", *ECCE2014*, Pittsburgh, Pennsylvania, USA, pp. 4513-4522, Sept. 2014.

[2] Y. Takano, M. Takeno, T. Imakawa, A. Chiba, N. Hoshi, M. Takemoto, S. Ogasawara, "Torque Density and Efficiency Improvements of a Switched Reluctance Motor Without Rare-Earth Material for Hybrid Vehicles", *ECCE2010*, pp. 2653-2659, Sept. 2010.

[3] M. Takeno, A. Chiba, N. Hoshi, S. Ogasawara, M. Takemoto, M. A. Rahman, "Test Results and Torque Improvement of the 50-kW Switched Reluctance Motor Designed for Hybrid Electric Vehicles", *IEEE Trans. on Industry Applications*, vol. 48, no. 4, pp. 1327-1334, July/Aug. 2012.

[4] M. Ferrari, N. Bianchi, A. Doria, E. Fornasiero, "Design of Synchronous Reluctance Motor for Hybrid Electric Vehicles", *IEMDC2013*, pp. 1058-1065, May 2013.

[5] M-F Hsieh, Y-C Hsu, D. G. Dorell, "Design of a Large-Power Surface-Mounted Permanent-Magnet Motors Using Postassembly Magnetization," , *IEEE Trans. on Industrial Electronics*, vol. 57, no. 10, pp. 3376-3384, Oct. 2010.

[6] A. G. Jack, B. C. Mecrow, P. G. Dickinson, D. Stephenson, J. S. Burdess, N. Fawcett, J. T. Evans, "Permanent-Magnet Machines with Powdered Iron Cores and Prepressed Windings" , *IEEE Trans. on Industry Applications*, vol. 36, no. 4, pp. 1077-1084, July/Aug. 2000.

[7] B-T Kim, "Design of New Type Universal Motor Using Soft Magnetic Composites" , *Journal of Electrical Engineering and Technology*, vol. 1, no. 2, pp. 211-115, 2006.

[8] R. Wrobel, P. H. Mellor, "Design Considerations of a Direct Drive Brushless Machine with Concentrated Windings", *IEEE Trans. on Energy Conversion*, vol. 23, no. 1, pp. 1-8, March 2008.

[9] R. Wrobel, P. H. Mellor, D. Holliday, "Thermal Modelling of a Segmented Stator Winding Design", *IEEE Trans. on Industry Applications*, vol. 47, no. 5, pp. 2023–2030, Sept./Oct. 2011.

[10] R. Wrobel, P. Mellor, N. McNeill, D.A. Staton, "Thermal Performance of an Open-Slot Modular-Wound Machine with External Rotor", *IEEE Trans. on Energy Conversion*, vol. 25, no. 2, pp. 403–411, 2010.

[11] R. Wrobel, D. Salt, N. Simpson, P. H. Mellor, "Comparative Study of Copper and Aluminium Conductors – Future Cost Effective PM Machines", *PEMD 2014*, Manchester, UK, pp. 1 -6, April 2014.

[12] J. D. Widmer, R. Martin, B.C .Mecrow, , "Pre-Compressed and Stranded Aluminium Motor Windings for Traction Motors," *IEMDC 2015*, pp.1851,1857, May 2015.

[13] J. Goss, R. Wrobel, P. H. Mellor, D. Staton, "The design of AC permanent magnet motors for electric vehicles: A design methodology", *IEMDC 2013*, 2013, pp. 871-878.

[14] R. Wrobel, D. Staton, R. Lock, J. Booker, D. Drury, "Winding Design for Minimum Power Loss and Low-Cost Manufacture in Application to Fixed-Speed PM Generator", *IEEE Tran. on Industry Applications*, (*early acess paper*).

[15] P. Mellor, R. Wrobel, D. Salt, A. Griffo, "Experimental and Analystical Determination of Proximity Losses in a High-Speed PM Machine", *ECCE2013*, pp. 3504-3511, September 2013.

[16] R. Wrobel, D. E. Salt, A. Griffo, N. Simpson, , P. H. Mellor, "Derivation and Scaling of Copper Loss in Thermal Modeling of Electrical Machines ", *IEEE Tran. on Industrial Electronics*, vol. 61, no. 8, pp. 4412 – 4420, August 2014.

[17] J. Goss, M. Popescu, D. Staton, R. Wrobel, J. Yon, P. Mellor, "A Comparision Between Maximum Torque/Ampere and Maximum Efficiency Control Strategies in IPM Synchronous Machines", *ECCE2014*, pp. 2403-2410, Sept. 2014.

[18] Motor-CAD V6 Maual, Motor Design Ltd, 2011.

[19] N. Simpson, R. Wrobel, P. Mellor, "Estimation of Equivalenet Thermal Parameters of Impregnated Electrical Windings," *IEEE Trans. on Industry Applications*, vol. 49, no. 6, pp. 2505 – 2515, Nov/Dec 2013.

[20] D. C. Hanselman, W. H. Peake, "Eddy-Currents Effects in Slot-Bound Conductors," *Electric Power Applications - IET Proceedings*, vol. 142, no. 2, pp. 131-136, 1995.